Mechanics of Advanced Composite Structures 4 (2017) 99-110

Mechanics of Advanced Composite Structures
journal homepage: http://MACS.journals.semnan.ac.ir

Semnan University

Vibration Optimization of Fiber-Metal Laminated Composite Shallow Shell Panels Using an Adaptive PSO Algorithm

H. Ghashochi-Bargh [a*], M.H. Sadr [b]

[a] *Department of Industrial, Mechanical and Aerospace Engineering, Buein Zahra Technical University, Buein Zahra, Qazvin, Iran*
[b] *Aerospace Engineering Department, Amirkabir University of Technology, Hafez Avenue, Tehran, Iran*

PAPER INFO

Paper history:
Received 2016-11-17
Revised 2017-04-04
Accepted 2017-04-11

Keywords:
Fiber metal laminate
Shallow shell
Optimization
Adaptive PSO algorithm

ABSTRACT

The paper illustrates the application of a combined adaptive particle swarm optimization (A-PSO) algorithm and the finite strip method (FSM) to the lay-up optimization of symmetrically fiber-metal laminated (FML) composite shallow shell panels for maximizing the fundamental frequency. To improve the speed of the optimization process, adaptive inertia weight was used in the particle swarm optimization algorithm to modify the search process. The use of the inertia weight provided a balance between global and local exploration and exploitation and resulted in fewer iterations on average to find an optimal solution. The fitness function was computed with a semi-analytical FSM. The number of layers, the fiber orientation angles, edge conditions, length/width (a/b) ratios, and length/radii of curvature (a/R) ratios were considered as design variables. The classical shallow shell theory (Donnell's formulation) was applied to calculate the natural frequencies of FML cylindrical curved panels. A program using Maple software was developed for this purpose. To check the validity, the obtained results were compared with some other stacking sequences. The numerical results of the proposed approach were also compared with other algorithms, which showed that the A-PSO algorithm provides a much higher convergence and reduces the required CPU time in searching for a global optimization solution. With respect to the first natural frequency and weight, a bi-objective optimization strategy for the optimal stacking sequence of FML panels is also presented using the weighted summation method.

DOI: 10.22075/MACS.2017.1744.1087

1. Introduction

Fiber-metal laminate (FML) composites are laminates composed of alternating layers of reinforced polymeric composites and aluminum alloys in such a way that the aluminum alloy sheets are outer layers that protect the inner composite layers. FMLs' main attribute is their improved fatigue resistance. Because of their outer aluminum alloy layers, FMLs have improved resistance to impacts and environmental conditions. The use of aluminum alloy layers improves specific stiffness and strength and also results in weight savings in the design of tension-dominated stresses in structural components. These hybrid materials are divided into three groups according to the type of fiber used in the polymeric composite layers, as follows: reinforced with aramid fibers (ARALL), glass fibers (GLARE), and carbon fibers (CARALL) [1, 2]. They have been introduced as structural composite materials for advanced aerospace applications, such as in the Airbus A380 aircraft fuselage, as aircraft lower wing skin, and as the internal parts of airplanes [3]. Figure 1 shows an FML-composite shallow shell panel structure that is discretized by strips. In aerospace applications, vibration can be a problem when the excitation frequency coincides with the resonance frequency, which is essential to maximize the fundamental frequency in laminated cylindrical panels.

* Corresponding author. Tel.: +98-9144088380

E-mail address: Ghashochi.b@bzte.ac.ir

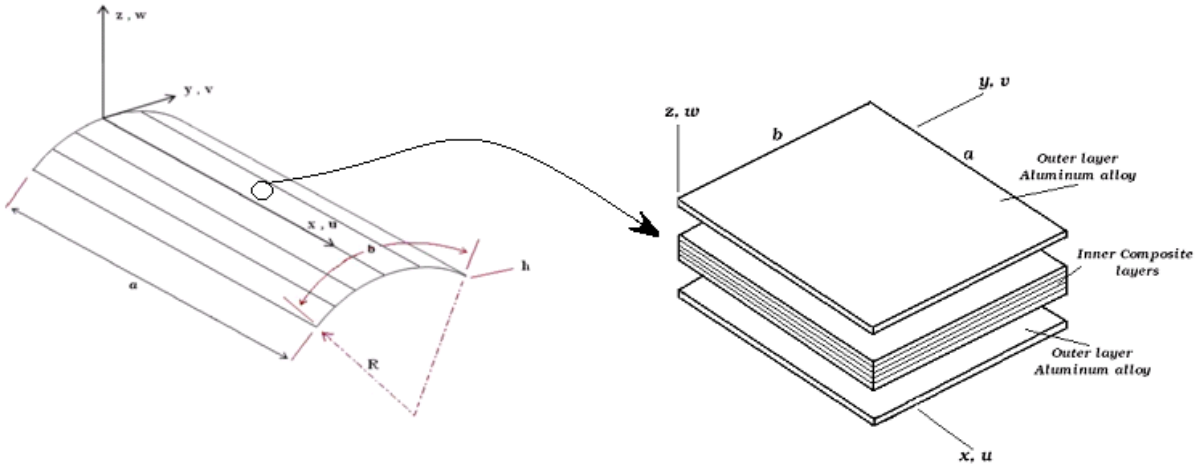

Figure 1. Cylindrical curved FML panel structure discretized by strips.

Several researchers have reported different studies on optimizing the natural frequency of laminated composite materials. Mateus et al. [4] studied the optimal design of thin, laminated plates and obtained results for the maximum fundamental frequency and minimum elastic strain energy using the finite element method to determine the frequency response. Narita [5] offered a Ritz-based layerwise optimization approach for symmetrical composite plates with respect to fiber orientation. Apalak et al. [6] determined the optimal layer sequences of symmetrical composite plates using a genetic algorithm, artificial neural networks, and the finite element method. The fundamental frequency optimization of laminated composite plates was studied by Ghashochi and Sadr [7, 8] using an elitist genetic algorithm, a particle swarm optimization (PSO) algorithm, and the finite strip method. They also studied the optimal design of FML plates and obtained results for the maximum fundamental frequency using a PSO algorithm [9]. Sumana et al. [10] investigated the effect of fiber orientation on the hydrostatic buckling behavior of a fiber-metal composite cylinder. Moniri Bidgoli and Heidari-Rarani [11] investigated the buckling behavior of an FML circular cylindrical shell under axial compression via both analytical and finite element approaches. They studied the effects of FML parameters such as metal volume fraction (MVF), composite fiber orientation, the stacking sequence of layers, and geometric parameters on the buckling loads. Topal [12] studied the frequency optimization of symmetrically laminated angle-ply annular sector plates using the first-order shear deformation theory and finite element method to investigate the effects of annularity, boundary conditions, and sector angles on the optimal designs. Nazari et al. [13] optimized the maximum natural frequencies of FMLs of cylindrical shells. They used first-order deformation theory and the double Fourier series to solve the free vibration problem.

The objective of the present study was to find the optimum stacking sequence of the inner composite layers of FML shallow shell panels that gives the maximum natural frequency using the adaptive PSO (A-PSO) algorithm and finite strip method. To improve the speed of the optimization process, an adaptive strategy was used in the PSO algorithm. The classical shallow shell theory (Donnell's formulation) was used for the finite strip formulation of the laminated shallow shell panels. Finally, the effect of different panel aspect ratios, ply angles, number of layers, and boundary conditions on the optimal designs was investigated.

2. Mathematical Modeling

The classical shallow shell theory (CST) was used to perform the analysis. In the CST, the constitutive equations for a shallow shell panel can be expressed by performing appropriate analytical integration through the uniform thickness, as follows [14]:

$$\begin{Bmatrix} N_x \\ N_y \\ N_{xy} \\ M_x \\ M_y \\ M_{xy} \end{Bmatrix} = \int_{-h/2}^{h/2} \begin{Bmatrix} \bar{\sigma}_x \\ \bar{\sigma}_y \\ \bar{\tau}_{xy} \\ z\bar{\sigma}_x \\ z\bar{\sigma}_y \\ z\bar{\tau}_{xy} \end{Bmatrix} .dz = \begin{bmatrix} A_{ij} & B_{ij} \\ B_{ij} & D_{ij} \end{bmatrix} \times \begin{Bmatrix} \varepsilon \\ \psi \end{Bmatrix}, \qquad (1a)$$

where N_x, N_y, and N_{xy} are the membrane direct and shearing stress resultants per unit length; M_x, M_y, and M_{xy} are the bending and twisting stress couples per unit length; and A_{ij}, B_{ij}, and D_{ij} are the matrices of stiffness coefficients. These matrices are defined by the following:

$$A_{ij}=\begin{bmatrix} A_{11} & A_{12} & A_{16} \\ A_{12} & A_{22} & A_{26} \\ A_{16} & A_{26} & A_{66} \end{bmatrix}, B_{ij}=\begin{bmatrix} B_{11} & B_{12} & B_{16} \\ B_{12} & B_{22} & B_{26} \\ B_{16} & B_{26} & B_{66} \end{bmatrix}, \quad D_{ij}=\begin{bmatrix} D_{11} & D_{12} & D_{16} \\ D_{12} & D_{22} & D_{26} \\ D_{16} & D_{26} & D_{66} \end{bmatrix} \tag{1b}$$

and ε and ψ are the in-plane strain vectors at the mid-plane and the curvature strain vector. They are defined by the following:

$$\varepsilon=\begin{Bmatrix} u_{,x} \\ v_{,y}+\dfrac{w}{R} \\ u_{,y}+v_{,x} \end{Bmatrix}, \psi=\begin{Bmatrix} -w_{,xx} \\ -w_{,yy} \\ -2w_{,xy} \end{Bmatrix}. \tag{1c}$$

The panel stiffness coefficients are defined as

$$(A_{ij},B_{ij},D_{ij})=\sum_{k=1}^{n}\int_{zk-1}^{zk}(\bar{Q}_{ij})_k(1,z,z^2)dz, \quad i,j=1,\ 2,\ 6 \tag{2}$$

Here, $(\bar{Q}_{ij})_k$ is the transformed reduced stiffness matrix. Due to the symmetry of the lay-up, the coupling between in-plane and out-of-plane force and deformations will not appear (i.e., $B_{ij}=0$).

The strain energy of the structure per unit volume is $1/2\,\bar{\sigma}^T\bar{\varepsilon}$. Using Equations (1) and (2) and integrating through the thickness of the structure with respect to z gives an expression for the strain energy of a finite strip, which can be put into the following form:

$$U_s=\frac{1}{2}\iint\{\varepsilon^T.[A].\varepsilon+\psi^T.[D].\psi\}dxdy$$
$$U_s=\frac{1}{2}\{d\}^T.[k].\{d\} \tag{3}$$

The general expression for the strip kinetic energy is:

$$T_s=\frac{1}{2}\rho h\iint\{\dot{u}^2+\dot{v}^2+\dot{w}^2\}dxdy=\frac{1}{2}\{\dot{d}\}^T.[m].\{\dot{d}\}, \tag{4}$$

where [k] is the strip stiffness matrix, [m] is the strip mass matrix, {d} is a column matrix that contains the strip's degrees of freedom, and ρ is the mean mass per unit area of the panel. For the whole structure, the total strain energy and kinetic energy are obtained by summations of the corresponding energy components of all strips.

The structural equation of motions can be obtained by applying the Lagrange equations as

$$[M].\{\ddot{\bar{d}}\}+[K].\{\bar{d}\}=\{0\}. \tag{5}$$

The solution of this eigenvalue problem is

$$\det([K]-\omega^2[M])=\{0\}, \tag{6}$$

where ω are the natural frequencies. The natural frequency is normalized as a frequency parameter in

$$\Omega=\omega a^2(\frac{\rho}{D_0})^{1/2}, \tag{7}$$

where the reference bending rigidity is

$$D_0=E_2h^3/12(1-\nu_{12}\nu_{21}). \tag{8}$$

The optimal design problem can be stated as follows:

$$\begin{aligned} &Find \quad \theta=(Al,\theta_1,\theta_2,...,\theta_k,Al) \\ &Maximize \quad \Omega=\Omega(\theta_1,\theta_2,...,\theta_k) \\ &Subject\ to \quad -90^0<\theta_n\le 90^0 \end{aligned} \tag{9}$$

where k, Al, and Θ are half of the inner composite layers' number, the number of aluminum layers, and the optimum ply angles, respectively. The optimal stacking sequences and ply angles were searched for with the A-PSO algorithm.

In the bi-objective optimization of FML panels, the objective functions combined with each other through the weighted summation method. The obtained single objective function was then optimized using A-PSO. To simultaneously maximize the fundamental natural frequency and minimize the weight, the objective function was considered to be in the form $f(\theta, Al)$ as a function of laminated angles and the sequence of metal and composite layers, which is defined as

$$f(\theta,Al)=W1\frac{\omega}{\omega_0}+W2\frac{(1/\sigma)}{(1/\sigma_0)} \tag{10}$$

where $W1$ and $W2$ are the weighting coefficients that sum the two objective functions to have a single fitness function, ω and σ are the optimum frequency and optimum weight, and ω_0 and σ_0 are the fundamental frequency and weight corresponding to the prescribed stacking sequences [Al/90/0/90]$_s$ [8].

In addition, the bi-objective optimization of FML panels is considered as follows:

$$\begin{aligned} &Maximize \quad \omega(\theta_n,Al) \\ &Minimize \quad \sigma(\theta_n,Al)=\sum_{k=1}^{N}\rho_k\times t_t\times A_k \\ &Subject\ to \quad -90^0<\theta_n\le 90^0 \text{ and sequence of metal and composite layers} \end{aligned} \tag{11}$$

where ρ, t, and A are density, thickness, and area of layers, respectively.

The assumed in-plane displacement and out-of-plane displacement in the full-energy semi-analytical finite strip method are

$$u=\sum_{i=1}^{ru}((1-\eta)u_{1i}+\eta u_{2i})\cos(i\zeta x)$$
$$v=\sum_{i=1}^{rv}((1-\eta)v_{1i}+\eta v_{2i})\sin(i\zeta x)$$
$$w=\sum_{i=1}^{rw}((1-3\eta^2+2\eta^3)w_{1i}+b_s(\eta-2\eta^2+\eta^3)\theta_{1i} \quad (12)$$
$$+(3\eta^2-2\eta^3)w_{2i}+b_s(\eta^3-\eta^2)\theta_{2i})W_i(x)$$
$$W_i(x)=\begin{cases}\sin(i\zeta x) & end\ simply\ \text{sup}\ ported\\ \sin(\zeta x).\sin(i\zeta x) & end\ clamped\end{cases}$$

where u_{1i}, u_{2i}, v_{1i}, and v_{2i} are the undetermined in-plane nodal displacement parameters; w_{1i}, w_{2i}, Θ_{1i}, and Θ_{2i} are the undetermined, out-of-plane nodal displacement parameters along the edges of the strip; $\eta=y/b_s$; and $\zeta=\pi/a$ [8, 9].

3. Adaptive Particle Swarm Optimization Algorithm

PSO is a population-based stochastic optimization technique developed by Eberhart and Kennedy in 1995 [15] inspired by the social behavior of animals, such as fish schooling, insects swarming, and birds flocking. This method is used to search for the global optimum of a wide variety of arbitrary problems. PSO shares many similarities with evolutionary computation techniques such as genetic algorithms (GA). However, unlike GA, PSO has no evolution operators such as crossover and mutation. Compared to GA, PSO is based on social biology, which requires cooperation, while GA is based on competition. The advantages of PSO are its simple structure, its immediate accessibility for practical applications, its ease of implementation, its speed to acquire solutions, and its robustness. In PSO, each single solution is a "bird" in the search space. We call it "particle." All of the particles have fitness values that are evaluated by the fitness function to be optimized and have velocities that direct the flight of the particles. The particles fly through the problem space by following the currently optimum particles.

PSO is initialized with a group of random particles and then searches for optima by updating generations. In every iteration, each particle is updated by following two "best" values. The first one (p^i) is the best position attained by the particle i in the swarm so far. Another best value (p_{k-1}^g) is the global best position attained by the swarm at iteration k-1. After finding the two best values, the basic swarm parameters of position and velocity are updated using the following equations at each iteration [16]:

$$v_k^i=v_{k-1}^i+c_1r_1(p^i-x_{k-1}^i)+c_2r_2(p_{k-1}^g-x_{k-1}^i), \quad (13)$$
$$x_k^i=x_{k-1}^i+v_k^i, \quad (14)$$

where the superscript i denotes the particle; the subscript k denotes the iteration number; v denotes the velocity; and x, which is a real number, denotes the position. The variables r_1 and r_2 are uniformly distributed random numbers in the interval [-1,1], and c_1 and c_2 are the acceleration constants. In a different reference, it is mentioned that the choice of these constants is problem-dependent. In this work, $c_1 = c_2 = 1$ was chosen, which gives optimal results in fewer iterations. The results were also rounded to the nearest integer values after optimization. A simple way to understand this updating procedure is described by Hassan, Cohanim, and Weck [17].

Since the initial development of PSO by Kennedy and Eberhart, several variants of this algorithm have been proposed by researchers. The first modification introduced in PSO was the use of an inertia weight parameter in the velocity update equation of the initial PSO, resulting in Equation (13), a PSO model that is now accepted as the global best PSO algorithm [18]. It is as follows:

$$v_i(t+1)=wv_i(t)+b_1r_1(x_i^{lb}-x_i(t))+b_2r_2(x^{gb}-x_i(t)) \quad (15)$$

In Eberhart and Shi's paper [19], a random value of inertia weight was used to enable the PSO to track the optima in a dynamic environment. It is difficult to predict whether a given time exploration (large values of w) or exploitation (small values of w) would be better in dynamic environments. So, a random value of w is selected to address this problem.

$$w=0.5+\frac{rand()}{2}, \quad (16)$$

where $rand()$ is a random number in [0,1] and w is then a uniform random variable in the range [0.5,1].

In the papers by Eberhart and Shi [20, 21], a linearly decreasing inertia weight was introduced and was shown to be effective in improving the fine-tuning characteristic of the PSO. In this method, the value of w is linearly decreased from an initial value of w to a final value of w according to the following equation:

$$w(iter)=\frac{iter_{\max}-iter}{iter_{\max}}(w_{\max}-w_{\min})+w_{\min}, \quad (17)$$

where $iter$ is the current iteration of the algorithm, and $iter_{max}$ is the maximum number of iterations the PSO is allowed to continue. This strategy is very common, and most of the PSO algorithms adjust the value of inertia weight using this updating scheme.

$$w=\left(\frac{2}{iter}\right)^{0.3}. \quad (18)$$

There are other approaches that use decreasing inertia weights [22], such as

In the present study, an adaptive strategy was used in the algorithm. In this strategy, a more diverse set of solutions generate near the best solutions so far until the end of each cycle in the algorithm. The use of an adaptive inertia weight provides a balance between global and local exploration and exploitation, and results in fewer iterations on average to find a sufficiently optimal solution. A parameter is defined to control the amount of generated solutions near the best solutions. In the algorithm, this parameter was assumed to be 20% of the best solutions. Thus, the same number of solutions will always be generated from a solution. As the value of the parameter increases, the PSO search becomes more localized. Thus, using a large value for the parameter may prevent the PSO from finding the global optimum. A selection procedure based on the fitness function picks the best solutions and replaces them in algorithm.

Adaptive inertia weight is updated using the following equation at each iteration [23]:

$$w=\frac{Fitness_{\min}}{Fitness_{\max}},\qquad 0<w\le 1, \tag{19}$$

where *Fitness* $_{min}$ is the minimum value of *Fitness* and *Fitness* $_{max}$ is the maximum value of *Fitness* in every iteration of the PSO.

Table 1. Test functions used in the paper were unimodal (U), multimodal (M), separable (S), and nonseparable (N).

No.	Function Name	Test Function	x_{min}	$f(x)_{min}$
1	Bohachevsky 1 (BO1, MS)	$f(x)=x_1^2+x_2^2-0.3\cos(3\pi x_1)-0.4\cos(4\pi x_2)+0.7,$ $subject\ to\ -100\le x_1,\ x_2\le 100$	(0,0)	0
2	Bohachevsky 2 (BO2, MN)	$f(x)=\sum_{i=1}^{n-1}x_i^2+2x_{i+1}^2-0.3\cos(3\pi x_i)\cos(4\pi x_{i+1})+0.3,$ $subject\ to\ -100\le x_i\le 100,\ i=1,...,n.$	(0,0)	0
3	Branin RCOS (RC, MN)	$f(x)=\left(x_2-\frac{5.1}{4\pi^2}x_1^2+\frac{5}{\pi}x_1-6\right)^2+10\left(1-\frac{1}{8\pi}\right)\cos(x_1)+10,$ $subject\ to\ -5\le x_1,x_2\le 15.$	$(-\pi,12.275),$ $(\pi,2.275),$ $(3\pi,2.475)$	$\frac{5}{4\pi}$
4	Easom (ES, UN)	$f(x)=-\cos(x_1)\cos(x_2)\exp(-(x_1-\pi)^2+(x_2-\pi)^2),$ $subject\ to\ -10\le x_1,x_2\le 10.$	(π,π)	-1
5	Goldstein and Price (GP, MN)	$f(x)=[1+(x_1+x_2+1)^2(19-14x_1+3x_1^2-14x_2+6x_1x_2+3x_2^2)]\times$ $[30+(2x_1-3x_2)^2(18-32x_1+12x_1^2+48x_2-36x_1x_2+27x_2^2)],$ $subject\ to\ -2\le x_1,x_2\le 2.$	(0,-1)	3
6	Six-hump Camel Back (SB,MN)	$f(x)=4x_1^2-2.1x_1^4+1/3x_1^6+x_1x_2-4x_2^2+4x_2^4,$ $subject\ to\ -5\le x_1,x_2\le 5.$	$(-0.0898,0.7126)$ $(0.0898,-0.7126)$	-1.03163
7	Shubert (SH, MN)	$f(x)=\left(\sum_{i=1}^{5}i\cos((i+1)x_1+i)\right)\left(\sum_{i=1}^{5}i\cos((i+1)x_2+i)\right),$ $subject\ to\ -10\le x_1,x_2\le 10.$	Include 760 local minimum	-186.730
8	Colville (CO, UN)	$f(x)=100(x_1^2-x_2)^2+(x_1-1)^2+(x_3-1)^2+90(x_3^2-x_4)^2+$ $10.1((x_2-1)^2+(x_4-1)^2)+19.8(x_2-1)(x_4-1),$ $subject\ to\ -10\le x_i\le 10,\ i=1,2,3,4.$	(1,1,1,1)	0
9	Michalewicz (MI, MS)	$f(x)=-\sum_{i=1}^{n}\sin(x_i)(\sin(ix_i^2/\pi))^{20},$ $subject\ to\ -0\le x_i\le \pi,\ i=1,...,n.$	Include $n!$ local minimum	-3.3223
10	Griewank (GR, MN)	$f(x)=\frac{1}{4000}\sum_{i=1}^{n}x_i^2-\prod_{i=1}^{n}\cos\left(\frac{x_i}{\sqrt{i}}\right)+1,$ $subject\ to\ -600\le x_i\le 600,\ i=1,...,n.$	(0,...,0)	0

To evaluate the proposed algorithm (A-PSO), it was compared with three other optimization algorithms. To investigate the performance of the optimization algorithms, ten benchmark test functions were adopted. Table 1 provides a detailed description of these functions.

The performance of the A-PSO is shown in Tables 2–5 in comparison with other algorithms for different parameters. From the tables, it can be inferred that for the ten test problems, A-PSO performed better than ABC and PSO in the case of nine problems. As seen from tables, the results obtained by A-PSO are closer to the results of RABC, whereas RABC performs better than A-PSO for five functions. In addition, it was concluded that using A-PSO provides a much higher convergence and reduces the required CPU time in comparison with the ABC and PSO algorithms.

Table 2. Search result comparisons on ten test functions.

No.	Function	Problem Dimension	Global Minimum	ABC [24]	RABC [24]	PSO	A-PSO
1	BO1	2	0	0	0	0	0
2	BO2	2	0	0	0	0	0
3	RC	2	0.397887	0.397887	0.397887	0.397887	0.397887
4	ES	2	-1	-1	-1	-1	-1
5	GP	2	3	3.000010	3	3.000071	3
6	SB	2	-1.03163	-1.03163	-1.03163	-1.03163	-1.03163
7	SH	2	-186.7309	-186.7309	-186.7309	-186.7309	-186.7309
8	CO	4	0	1.6073e-1	1.1989e-27	1.7965e-6	1.0165e-39
9	MI	10	-9.66015	-9.66015	-9.66015	-9.66015	-9.66015
10	GR	30	0	0	0	0	0

Table 3. The standard deviation of the best solutions on ten test functions.

No.	Function	Problem Dimension	ABC [24]	RABC [24]	PSO	A-PSO
1	BO1	2	0	0	0	0
2	BO2	2	0	0	0	0
3	RC	2	3.3650e-16	3.3650e-16	3.4742e-16	3.3054e-16
4	ES	2	0	0	0	0
5	GP	2	3.7232e-5	8.9720e-16	7.3722e-9	2.7544e-15
6	SB	2	2.2430e-16	2.3093e-16	2.3151e-16	2.005e-16
7	SH	2	1.1613e-13	7.4204e-14	9.0177e-11	8.1951e-14
8	CO	4	1.0917e-1	3.3911e-27	4.8217e-6	3.217e-31
9	MI	10	3.5888e-16	5.0753e-16	7.4301e-16	3.5190e-16
10	GR	30	0	0	0	0

Table 4. Number of functions evaluated for optimization with different algorithms on ten test functions.

No.	Function	Problem Dimension	ABC [24]	RABC [24]	PSO	A-PSO
1	BO1	2	1998	500	1216	428
2	BO2	2	2625	656	1950	537
3	RC	2	1608	72	432	86
4	ES	2	3314	989	2864	1578
5	GP	2	27773	326	1953	723
6	SB	2	854	239	940	214
7	SH	2	2114	465	3007	512
8	CO	4	-	1031	4906	686
9	MI	10	25381	26380	29587	27870
10	GR	30	56555	32168	50331	30431

Table 5. Comparison of CPU time for different algorithms on ten test functions.

No.	Function	Problem Dimension	ABC [24]	RABC [24]	PSO	A-PSO
1	BO1	2	0.093	0.031	0.068	0.022
2	BO2	2	0.109	0.031	0.083	0.026
3	RC	2	0.093	0.015	0.046	0.016
4	ES	2	0.218	0.094	0.198	0.122
5	GP	2	0.953	0.015	0.081	0.039
6	SB	2	0.062	0.031	0.064	0.030
7	SH	2	0.156	0.046	0.213	0.062
8	CO	4	16.28	0.109	0.280	0.088
9	MI	10	3.718	3.921	4.455	3.935
10	GR	30	8.625	5.281	8.197	5.149

4. Results and Discussions

The fundamental frequency of hybrid laminates was maximized for different panel aspect ratios, ply angles, length/R (a/R) ratios, number of layers, and boundary conditions. The degree of panel curvature was taken as a/R = 0 (plate), a/R = 0.2 (relatively shallow), and a/R = 0.5 (shallow) in the examples. A rise in the center was only 3% of the radius R for a shell of a/R = 0.5, and this can be regarded as geometry within the shallow shell theory [25–27]. The laminates were symmetric and made of AS/3501 graphite/epoxy material [28] (inner composite layers) and aluminum alloy 2024-T3 [1] (outer aluminum layers). The material properties of the lamina are given as follows: for the composite layers, E_1 = 138 GPa, E_2 = 8.96 GPa, G_{12} = 7.1 GPa, and υ_{12} = 0.3; and for the aluminum layers, E = 72.4 GPa and υ = 0.33. Each of the lamina was assumed to be same thickness.

In Table 6, the optimization of composite laminated panels using the PSO algorithm was validated with those given by Narita [5] through the use of the Ritz-based layerwise optimization method. As seen, the PSO algorithm was successful in predicting the optimal solutions, and higher natural frequencies than those predicted by Narita were achieved for different edge conditions. It can also be seen in Table 7 that there was a very good agreement between the results of the present approach and the published paper by Shooshtari and Razavi [1] for the fundamental frequency of symmetric FML panels (Glare 3). The lay-up and material properties of this hybrid composite (Glare 3) are as follows [1]:
Al(2024-T3)/[0^0/90^0]GFRC/Al(2024-T3)/[90^0/0^0]GFRC/Al(2024-T3)
Glass fiber–reinforced composite layers (0.2 mm thickness each): E_1 = 55.8979 GPa, E_2 = 13.7293 GPa, G_{12} = 5.5898 GPa, υ_{12} = 0.277, and ρ = 2550 kg/m^3
Aluminum alloy 2024-T3 layers (0.3 mm thickness each): E = 72.4 GPa, υ = 0.33, and ρ = 2700 kg/m^3

The dimensionless fundamental frequency of Glare 3 was obtained by using the following equation:

$$\Omega = \omega a^2 \left(\frac{I_0}{D_{11}}\right)^{1/2}, \tag{20}$$

where $I_0 = \int_{-\frac{h}{2}}^{\frac{h}{2}} \rho dz$ is the mass moment of inertia.

The accuracy of the A-PSO in predicting the optimal solutions is shown in Figure 2 in comparison with other stacking sequences with various aspect ratios when the length/R = 0.5. The comparisons demonstrate that the panels with the present optimum lay-ups actually give higher fundamental frequencies than panels with other lay-ups. The typical stacking sequences of symmetric 10-layer FML-composite shallow panels were chosen for comparison purposes; namely, [Al/0/0/0/0]$_S$, [Al/30/-30/30/-30]$_S$, and [Al/45/-45/45/-45]$_S$.

The optimal layered sequences and maximal natural frequency parameters of symmetric FML shallow shell panels were searched for using A-PSO for the various combinations of free (F), simply supported (S), and clamped (C) edge conditions. The panel length/width ratios (a/b = 1, 2, 3, 4), length/R (a/R = 0, 0.2, 0.5), and the layer number (n = 6, 10) are given in Tables 8, 9, and 10. The fiber angle of each inner ply in the FML-composite shallow shell panels was changed with a step of $\Delta\theta = 1^0$ between $-90^0 < \theta_n \leq 90^0$.

Table 6. Comparison of the optimal stacking sequences and natural frequency parameter of symmetric eight-layered composite panels (a/b = 2, increment 1^0).

Case	Edges BCs	Ω_{opt}		Optimal stacking	
		Narita [5]	Present study	Narita [5]	Present study
1	SFSF	38.66	38.661	[0/0/0/0]s	[0/0/0/0]s
2	SSSF	45.26	48.575	[0/-30/40/35]s	[-38/38/37/37]s
3	SCSF	61.94	64.203	[90/70/-55/-55]s	[60/59/-61/60]s
4	SSSS	159.9	159.886	[90/90/90/90]s	[90/90/-89/90]s
5	SSSC	245.7	245.736	[90/90/90/90]s	[90/90/90/90]s
6	SCSC	353.9	353.943	[90/90/90/90]s	[90/90/90/90]s

Table 7. Dimensionless frequencies of rectangular Glare 3–hybrid composite (h/a = 0.01).

BCs	a/b	Ω	
		Shooshtari and Razavi [1]	Present study
SSSS	1	19.4723	19.541
	4/3	26.9917	27.135
	2	48.5124	48.597

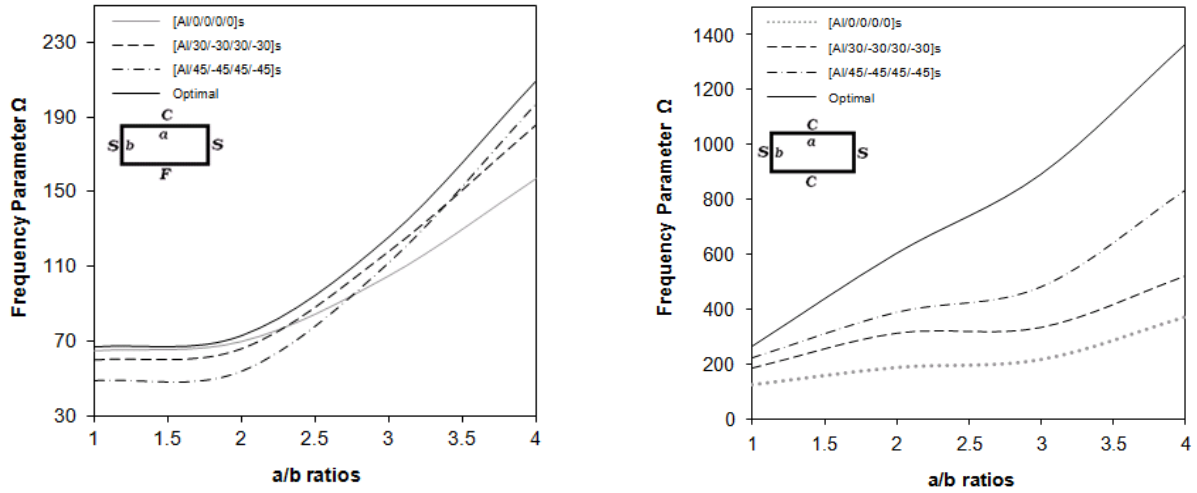

Figure 2. Comparison between the optimal natural frequency parameters Ω_{opt} and the natural frequency parameter of symmetric FML ten-layered shallow panels for various stacking sequences, a/b ratios, and edge conditions ([a] SCSF, [b] SCSC) when a/R = 0.5.

Table 8. Optimum solutions for symmetric, fiber-metal laminated, shallow shell–type panels for different *a/b* ratios and edge conditions when $a/R = 0.5$.

Number of laminae:		6		10	
BCs	a/b	$[Al/\theta_1/\theta_2]_{S,opt}$	Ω_{opt}	$[Al/\theta_1/\theta_2/\theta_3/\theta_4]_{S,opt}$	Ω_{opt}
SFSF	1	$[Al/-36/86]_S$	61.962	$[Al/9/-55/73/-81]_S$	60.098
	2	$[Al/1/-20]_S$	55.407	$[Al/0/10/-20/33]_S$	56.263
	3	$[Al/1/-20]_S$	38.528	$[Al/0/-5/13/-19]_S$	40.619
	4	$[Al/1/-17]_S$	33.939	$[Al/-2/5/0/17]_S$	36.327
SSSF	1	$[Al/-73/89]_S$	67.171	$[Al/35/90/84/90]_S$	66.062
	2	$[Al/-31/90]_S$	79.009	$[Al/-36/-62/-13/86]_S$	79.087
	3	$[Al/-45/90]_S$	73.375	$[Al/-40/47/90/90]_S$	67.698
	4	$[Al/-45/90]_S$	84.962	$[Al/-46/49/90/90]_S$	85.158
SCSF	1	$[Al/-31/90]_S$	55.126	$[Al/32/90/90/90]_S$	67.176
	2	$[Al/90/90]_S$	76.847	$[Al/90/90/90/90]_S$	73.164
	3	$[Al/90/90]_S$	123.926	$[Al/90/90/90/90]_S$	126.083
	4	$[Al/90/90]_S$	201.713	$[Al/90/90/90/90]_S$	209.647
SSSS	1	$[Al/-68/-63]_S$	244.345	$[Al/-69/-64/-66/-63]_S$	243.382
	2	$[Al/90/90]_S$	538.297	$[Al/90/90/90/90]_S$	566.376
	3	$[Al/90/90]_S$	642.306	$[Al/90/90/90/90]_S$	666.099
	4	$[Al/90/90]_S$	776.600	$[Al/90/90/90/90]_S$	811.081
SSSC	1	$[Al/76/-65]_S$	248.071	$[Al/90/-78/64/-62]_S$	247.557
	2	$[Al/90/90]_S$	569.830	$[Al/90/90/90/90]_S$	591.029
	3	$[Al/90/90]_S$	712.090	$[Al/90/90/90/90]_S$	743.592
	4	$[Al/90/90]_S$	979.027	$[Al/90/90/90/90]_S$	1031.343
SCSC	1	$[Al/90/-86]_S$	255.741	$[Al/90/90/90/-66]_S$	263.052
	2	$[Al/90/90]_S$	597.414	$[Al/90/90/90/90]_S$	601.425
	3	$[Al/90/90]_S$	845.220	$[Al/90/90/90/90]_S$	888.938
	4	$[Al/90/90]_S$	1285.370	$[Al/90/90/90/90]_S$	1362.087

Table 9. Optimum solutions for symmetric, fiber-metal laminated, shallow shell–type panels for different *a/b* ratios and edge conditions when $a/R = 0.2$.

Number of laminae:		6		10	
BCs	a/b	$[Al/\theta_1/\theta_2]_{S,opt}$	Ω_{opt}	$[Al/\theta_1/\theta_2/\theta_3/\theta_4]_{S,opt}$	Ω_{opt}
SFSF	1	$[Al/-11/53]_S$	50.154	$[Al/10/33/-32/-68]_S$	50.237
	2	$[Al/0/-15]_S$	36.318	$[Al/-2/8/1/-36]_S$	38.343
	3	$[Al/-1/2]_S$	32.696	$[Al/2/0/-1/2]_S$	34.955
	4	$[Al/-1/2]_S$	31.815	$[Al/0/-3/-2/-1]_S$	34.046
SSSF	1	$[Al/-35/80]_S$	54.373	$[Al/-34/37/90/90]_S$	53.274
	2	$[Al/-40/-14]_S$	56.645	$[Al/37/29/-23/90]_S$	56.247
	3	$[Al/44/-85]_S$	65.419	$[Al/-42/35/-45/2]_S$	67.698
	4	$[Al/-44/50]_S$	83.503	$[Al/-45/44/-41/51]_S$	85.337
SCSF	1	$[Al/-31/90]_S$	55.126	$[Al/9/-55/73/-81]_S$	53.242
	2	$[Al/-67/90]_S$	68.091	$[Al/-64/90/90/90]_S$	66.634
	3	$[Al/90/90]_S$	121.698	$[Al/90/90/90/90]_S$	124.253
	4	$[Al/90/90]_S$	200.984	$[Al/90/90/90/90]_S$	209.022
SSSS	1	$[Al/90/62]_S$	166.114	$[Al/90/90/90/-56]_S$	166.312
	2	$[Al/90/90]_S$	269.944	$[Al/90/90/90/90]_S$	278.449
	3	$[Al/90/90]_S$	382.736	$[Al/90/90/90/90]_S$	398.740
	4	$[Al/90/90]_S$	579.362	$[Al/90/90/90/90]_S$	609.558
SSSC	1	$[Al/90/-87]_S$	188.629	$[Al/90/90/90/90]_S$	192.639
	2	$[Al/90/90]_S$	305.173	$[Al/90/90/90/90]_S$	317.146
	3	$[Al/90/90]_S$	513.938	$[Al/90/90/90/90]_S$	541.148
	4	$[Al/90/90]_S$	845.157	$[Al/90/90/90/90]_S$	895.729
SCSC	1	$[Al/90/90]_S$	220.527	$[Al/90/90/90/90]_S$	227.478
	2	$[Al/90/90]_S$	367.400	$[Al/90/90/90/90]_S$	385.163
	3	$[Al/90/90]_S$	697.862	$[Al/90/90/90/90]_S$	739.480
	4	$[Al/90/90]_S$	1193.332	$[Al/90/90/90/90]_S$	1269.318

Table 10. Optimum solutions for symmetric, fiber-metal laminated, shallow shell-type panels for different *a/b* ratios and edge conditions when $a/R = 0$.

Number of laminae:		6		10	
BCs	a/b	$[Al/\theta_1/\theta_2]_{S,opt}$	Ω_{opt}	$[Al/\theta_1/\theta_2/\theta_3/\theta_4]_{S,opt}$	Ω_{opt}
SFSF	1	$[Al/0/0]_S$	33.014	$[Al/0/0/1/0]_S$	34.557
	2	$[Al/0/0]_S$	32.961	$[Al/0/0/0/2]_S$	34.380
	3	$[Al/0/0]_S$	33.925	$[Al/0/0/0/0]_S$	34.442
	4	$[Al/0/0]_S$	33.913	$[Al/0/0/0/0]_S$	34.317
SSSF	1	$[Al/0/0]_S$	36.893	$[Al/0/0/0/0]_S$	38.003
	2	$[Al/37/-39]_S$	47.796	$[Al/37/37/-37/-37]_S$	48.376
	3	$[Al/42/-46]_S$	65.772	$[Al/-41/44/-44/43]_S$	67.801
	4	$[Al/43/-44]_S$	83.184	$[Al/44/-44/45/45]_S$	88.031
SCSF	1	$[Al/0/1]_S$	38.748	$[Al/0/0/0/-2]_S$	39.323
	2	$[Al/58/64]_S$	65.319	$[Al/58/58/63/67]_S$	66.118
	3	$[Al/90/-89]_S$	128.007	$[Al/90/-88/90/90]_S$	129.554
	4	$[Al/90/90]_S$	206.413	$[Al/90/90/90/-88]_S$	208.195
SSSS	1	$[Al/-45/-46]_S$	56.777	$[Al/-45/-45/-45/44]_S$	56.229
	2	$[Al/-89/90]_S$	154.116	$[Al/90/90/90/90]_S$	154.807
	3	$[Al/90/88]_S$	343.068	$[Al/90/-88/90/-87]_S$	346.044
	4	$[Al/-89/89]_S$	552.521	$[Al/90/90/89/88]_S$	561.070
SSSC	1	$[Al/60/60]_S$	69.144	$[Al/60/60/60/59]_S$	69.331
	2	$[Al/88/90]_S$	222.937	$[Al/89/90/90/88]_S$	230.922
	3	$[Al/90/-89]_S$	520.766	$[Al/90/90/89/87]_S$	525.538
	4	$[Al/90/90]_S$	858.658	$[Al/89/90/-88/88]_S$	867.609
SCSC	1	$[Al/89/-89]_S$	88.997	$[Al/90/90/-89/-88]_S$	89.114
	2	$[Al/89/90]_S$	312.400	$[Al/90/90/-87/90]_S$	325.548
	3	$[Al/90/90]_S$	742.618	$[Al/90/90/90/-89]_S$	747.503
	4	$[Al/90/90]_S$	1218.994	$[Al/90/89/-88/90]_S$	1232.896

Table 11. Bi-objective optimization results of symmetric, FML, eight-layered panel (a = 1 m, b = 1 m).

W1	W2	ω (Hz)	σ (kg)	Optimum stacking sequences
0	1	6.8	5.1	[-45/45/45/-45]$_S$
0.25	0.75	8.94	5.175	[Al/-45/45/45]$_S$
0.5	0.5	9.8	5.25	[Al/Al/-45/45]$_S$
0.75	0.25	10.058	5.325	[Al/Al/Al/-45]$_S$
1	0	10.058	5.325	[Al/Al/Al/-45]$_S$

As can be seen, the optimal fiber orientations vary from 0^0 to 90^0 or 0^0 to -90^0 with increases in a/b ratios. The results demonstrate that the edge conditions play an important role in the natural frequency parameter of shallow FMLs. As the number of the clamped panel edges increased, an evident increase in the natural frequency parameters was observed. This can be explained by the fact that the clamped edges provide less degrees of freedom, and the effect of this is to stiffen the shallow panels. Since graphite/epoxy is far less dense than aluminum, the presented optimum FML results with two aluminum layers are optimum in terms of weight, too.

The results of the bi-objective optimization of symmetric, FML, eight-layered panels with simply supported edge conditions are presented in Table 11 with respect to the first natural frequency and the weight for a/b = 1 and a/R = 0. The laminates were made of glass fiber–reinforced composite [1] and aluminum alloy 2024-T3 [1], and the thickness of layers was considered to be 0.25 mm. As inferred from the results, the angle of layers and sequence of metal and composite layers play an important role in the fundamental frequency and weight of panels. As seen, FML panels with outer aluminum layers have the maximum natural frequency and minimum weight in comparison with other stacking sequences.

3. Conclusions

In this study, the fundamental frequency optimization of FML curved panels was studied using the combination of A-PSO and FSM for various panels edge conditions, a/b ratios, a/R ratios, and layer numbers. As inferred from the results, the A-PSO provides a much higher convergence and reduces the required CPU time in comparison with the PSO and ABC algorithms. As seen, the combination of A-PSO and FSM was successful in determining the fundamental frequency and the optimal layering sequences of FML curved panels. It can be noticed from the results that the maximum fundamental frequency and the optimum stacking sequences were substantially influenced by edge conditions, a/b ratios, and a/R ratios. The maximum fundamental frequency and the optimum fiber orientations were not substantially influenced and approach a limiting value with an increasing layer number.

References

[1] Shooshtari A, Razavi S. A closed form solution for linear and nonlinear free vibrations of composite and fiber metal laminated rectangular plates. *Compos Struct* 2010; 92: 2663-75.

[2] Botelho EC, Campos AN, Barros E, Pardini LC, Rezende MC. Damping behavior of continuous fiber/metal composite materials by the free vibration method. *Compos: Part B* 2006; 37: 255-63.

[3] Botelho EC, Almeida LC, Rezende MC. Elastic properties of hygrothermally conditioned glare laminate. *Int J Eng Sci* 2007; 45: 163-72.

[4] Mateus HC, Soares CMM, Soares CAM. Sensitivity analysis and optimal design of thin laminated composite structures. *Computers &Structures* 1991; 41: 501-8.

[5] Narita Y. Layerwise optimization for the maximum fundamental frequency of laminated composite plates. *J Sound and Vibration* 2003; 263: 1005-16.

[6] Apalak MK, Yildirim M, Ekici R. Layer optimisation for maximum fundamental frequency of laminated composite plates for different edge conditions. Composites *Science and Technology* 2008; 68: 537-50.

[7] Ghashochi Bargh H, Sadr MH. Stacking sequence optimization of composite plates for maximum fundamental frequency using particle swarm optimization algorithm. *Meccanica* 2012; 47: 719-30.

[8] Sadr MH, Ghashochi Bargh H. Optimization of laminated composite plates for maximum fundamental frequency using Elitist-Genetic algorithm and finite strip method. *J Glob Optim* 2012; 54: 707-28.

[9] Ghashochi-Bargh H, Sadr MH. A modified multi-objective elitist-artificial bee colony algorithm for optimization of smart FML panels. *Structural Engineering and Mechanics* 2014; 52(6): 1209-1224.

[10] Sumana BG, Sagar HV, Sharma KV, Krishna M. Numerical analysis of the effect of fiber orientation on hydrostatic buckling behavior of fiber

metal composite cylinder. *Journal of Reinforced Plastics and Composites* 2015; 34(17): 1422-1432.

[11] Moniri Bidgoli AM, Heidari-Rarani M. Axial buckling response of fiber metal laminate circular cylindrical shells. *Structural Engineering and Mechanics* 2016; 57(1): 45-63.

[12] Topal U. Frequency optimization of laminated composite annular sector plates. *Journal of Vibration and Control* 2015; 21(2): 320-327.

[13] Nazari A, Malekzade Fard K, Majidian M. Vibration analysis of FML cylindrical shell optimized according to maximum natural frequency under various boundary conditions. *Modares Mechanical Engineering* 2016; 16(7): 143-152.

[14] Narita Y, Robinson P. Maximizing the fundamental frequency of laminated cylindrical panels using layerwise optimization. *Int J Mech Sci* 2006; 48: 1516-24.

[15] Eberhart RC, Kennedy J. A new optimizer using particle swarm theory. In: Proceedings of the sixth international symposium on micro machine and human science, Nagoya, Japan. IEEE Service Center, Piscataway; 1995. p. 39–43.

[16] Eberhart RC, Shi Y. Comparison between genetic algorithms and Particle Swarm Optimization. In: Porto VW, Saravanan N, Waagen D and Eiben AE (eds) Evolutionary Programming VII, Springer; 1998. p. 611-16.

[17] Hassan R, Cohanim B, Weck O. A comparison of particle swarm optimization and the genetic algorithm. In: 46th AIAA/ASME/ASCE/AHS/ASC structures, structural dynamics & material conference, Austin, Texas; 2005. no. 1897.

[18] Shi Y, Eberhart R. Fuzzy adaptive particle swarm optimization. In: Congress on Evolutionary Computation, Seoul, Korea; 2001.

[19] Eberhart R.C, Shi Y.H, Tracking and optimizing dynamic systems with particle swarms. In: Congress on Evolutionary Computation, Korea; 2001.

[20] Shi Y.H, Eberhart RC. Empirical study of particle swarm optimization. In: Congress on Evolutionary Computation, Washington DC, USA; 1999.

[21] Shi Y.H, Eberhart R.C. Experimental study of particle swarm optimization. In: SCI2000 Conference, Orlando; 2000.

[22] Fan S, Chiu Y. A decreasing inertia weight particle swarm optimizer. *Engineering Optimization* 2007; 39: 203–228.

[23] Ghashochi-Bargh H, Khalili M, Mirzakarimi-Isfahani S. An Elitist Adaptive Particle Swarm Optimization Algorithm for Numerical Optimization. *Journal of Computational Intelligence and Electronic Systems* 2014; 3(4): 302-306.

[24] Kang F, Li J, Ma Zh. Rosenbrock artificial bee colony algorithm for accurate global optimization of numerical functions. *Information Sciences* 2011; 181: 3508-31.

[25] Avramov, KV, Papazov SV, Breslavsky ID. Dynamic instability of shallow shells in three-dimensional incompressible inviscid potential flow. *Journal of Sound and Vibration* 2017; 394: 593-611.

[26] Kar VR, Mahapatra TR, Panda SK. Effect of different temperature load on thermal postbuckling behaviour of functionally graded shallow curved shell panels. *Composite Structures* 2017; 160: 1236-1247.

[27] Narita, Y, Robinson P. Maximizing the fundamental frequency of laminated cylindrical panels using layerwise optimization. *International Journal of Mechanical Sciences* 2006; 48(12): 1516-1524.

[28] Vinson JR, Sierakowski RL. **The behavior of structures composed of composite materials.** Dordrecht: Martinus Nijhoff; 1986.